# A COMPUTER STUDY OF HYPERSONIC LAMINAR

# BOUNDARY-LAYER/SHOCK-WAVE INTERACTION

# USING THE TIME-DEPENDENT COMPRESSIBLE

# NAVIER-STOKES EQUATIONS

VON KÁRMÁN GAS DYNAMICS FACILITY
ARNOLD ENGINEERING DEVELOPMENT CENTER
AIR FORCE SYSTEMS COMMAND
ARNOLD AIR FORCE STATION, TENNESSEE 37389

September 1976

Final Report for Period July 1974 — April 1976

Prepared for

DIRECTORATE OF TECHNOLOGY (DY)
ARNOLD ENGINEERING DEVELOPMENT CENTER
ARNOLD AIR FORCE STATION, TENNESSEE 37389

This report has been reviewed by the Information Office (OI) and is releasable to the National Technical Information Service (NTIS). At NTIS, it will be available to the general public, including foreign nations.

## APPROVAL STATEMENT

This technical report has been reviewed and is approved for publication.

FOR THE COMMANDER

ELTON R. THOMPSON
Research & Development
   Division
Directorate of Technology

ROBERT O. DIETZ
Director of Technology

| REPORT DOCUMENTATION PAGE | | READ INSTRUCTIONS BEFORE COMPLETING FORM |
|---|---|---|
| 1 REPORT NUMBER<br>AEDC-TR-76-119 | 2 GOVT ACCESSION NO. | 3 RECIPIENT'S CATALOG NUMBER |
| 4 TITLE (and Subtitle)<br>A COMPUTER STUDY OF HYPERSONIC LAMINAR BOUNDARY-LAYER/SHOCK-WAVE INTERACTION USING THE TIME-DEPENDENT COMPRESSIBLE NAVIER-STOKES EQUATIONS | | 5 TYPE OF REPORT & PERIOD COVERED<br>Final Report - July, 1974 April 1976 |
| | | 6 PERFORMING ORG REPORT NUMBER |
| 7 AUTHOR(s)<br>B. K. Hodge - ARO, Inc. | | 8 CONTRACT OR GRANT NUMBER(s) |
| 9 PERFORMING ORGANIZATION NAME AND ADDRESS<br>Arnold Engineering Development Center (DY)<br>Air Force Systems Command<br>Arnold Air Force Station, Tennessee 37389 | | 10 PROGRAM ELEMENT PROJECT TASK AREA & WORK UNIT NUMBERS<br>Program Element 65807F |
| 11 CONTROLLING OFFICE NAME AND ADDRESS<br>Arnold Engineering Development Center(DYFS)<br>Air Force Systems Command<br>Arnold Air Force Station, Tennessee 37389 | | 12 REPORT DATE<br>September 1976 |
| | | 13 NUMBER OF PAGES 45 |
| 14 MONITORING AGENCY NAME & ADDRESS(if different from Controlling Office) | | 15 SECURITY CLASS (of this report)<br>UNCLASSIFIED |
| | | 15a DECLASSIFICATION DOWNGRADING SCHEDULE N/A |

16 DISTRIBUTION STATEMENT (of this Report)

Approved for public release; distribution unlimited.

17 DISTRIBUTION STATEMENT (of the abstract entered in Block 20, if different from Report)

18 SUPPLEMENTARY NOTES

Available in DDC

19 KEY WORDS (Continue on reverse side if necessary and identify by block number)

computers
shock wave-boundary layer interaction
laminar boundary layer
hypersonic flow

mathematical analysis
experimental data
numerical methods

20 ABSTRACT (Continue on reverse side if necessary and identify by block number)

This report presents the results of an investigation of hypersonic laminar boundary-layer/shock-wave interactions using the method of MacCormack to solve the time-dependent compressible Navier-Strokes equations. Comparisons of the numerical solutions with experimental data were made to ascertain the validity of the numerical method and to identify regions of anomalous behavior. The algorithm gave good results when applied to hypersonic laminar

DD $_{1 \, \text{JAN} \, 73}^{\text{FORM}}$ 1473   EDITION OF 1 NOV 65 IS OBSOLETE

**20.** ABSTRACT (Continued)

interactions that caused either small or no separated regions and marginal performance when applied to hypersonic laminar inter- actions having large regions of separated flow. The extents of the separated regions in interactions having large regions of separated flow were underpredicted when compared with experimental data. The predicted wall heat-transfer rates exhibited the correct quali- tative trend but not the experimentally measured quantitative values. Consideration of the effects of needed stabilizing terms as well as grid resolution suggests inadequate mesh spacing in the longitudinal direction as the cause of the aforementioned anom- alies. If inadequate mesh spacing (and the corresponding lack of support for every term of the Navier-Stokes equations) is a prime cause of the cited discrepancies between the numerical results and the experimental data, then the needed reduction of several orders of magnitude in $\Delta x$ would increase CPU time and core storage re- quirements to untenable levels.

## PREFACE

# CONTENTS

# ILLUSTRATIONS

**TABLE**

# 1.0 INTRODUCTION

The interaction of an oblique shock wave with a boundary layer is a phenomenon of considerable interest and frequent occurrence in supersonic and hypersonic flows. The effects of shock-wave impingement from externally carried aircraft stores on the aircraft and the effects of shock impingement from the aircraft on external stores have long been of interest to the military. Vehicles such as the TITAN IIIC and the Space Shuttle have geometries that make consideration of boundary-layer/shock-wave interaction a necessity. Numerous experimental studies have been undertaken to study, correlate, and explain the phenomenological aspects of the interaction problem. Concurrent with the interest shown by experimentalists in the boundary-layer/shock-wave interaction problem, much effort has been expended to develop theoretical techniques capable of accurately predicting the salient features of the problem.

The complexity of the interaction between a shock wave and a boundary layer gives rise to phenomena not characteristic of either a shock wave or a boundary layer. Figure 1 schematically illustrates the physics of a typical boundary-layer/shock-wave interaction. The boundary-layer equations are parabolic and hence can be integrated (at least to a point near separation) in a step-by-step downstream fashion once an impressed pressure gradient is specified. The boundary-layer/shock-wave interaction problem is not parabolic since the impressed pressure gradient is determined in part by the response of the boundary layer to the shock wave. Hence no a priori computation of the pressure is possible. Moreover, since separation and reattachment is a possibility, conventional boundary-layer methods cannot be used because a square-root-type singularity exists at separation for the boundary-layer equations. Thus, any solution technique must appeal to a system of governing equations more fundamental than either the Euler equations for inviscid flow or the boundary-layer equations. The more general Navier-
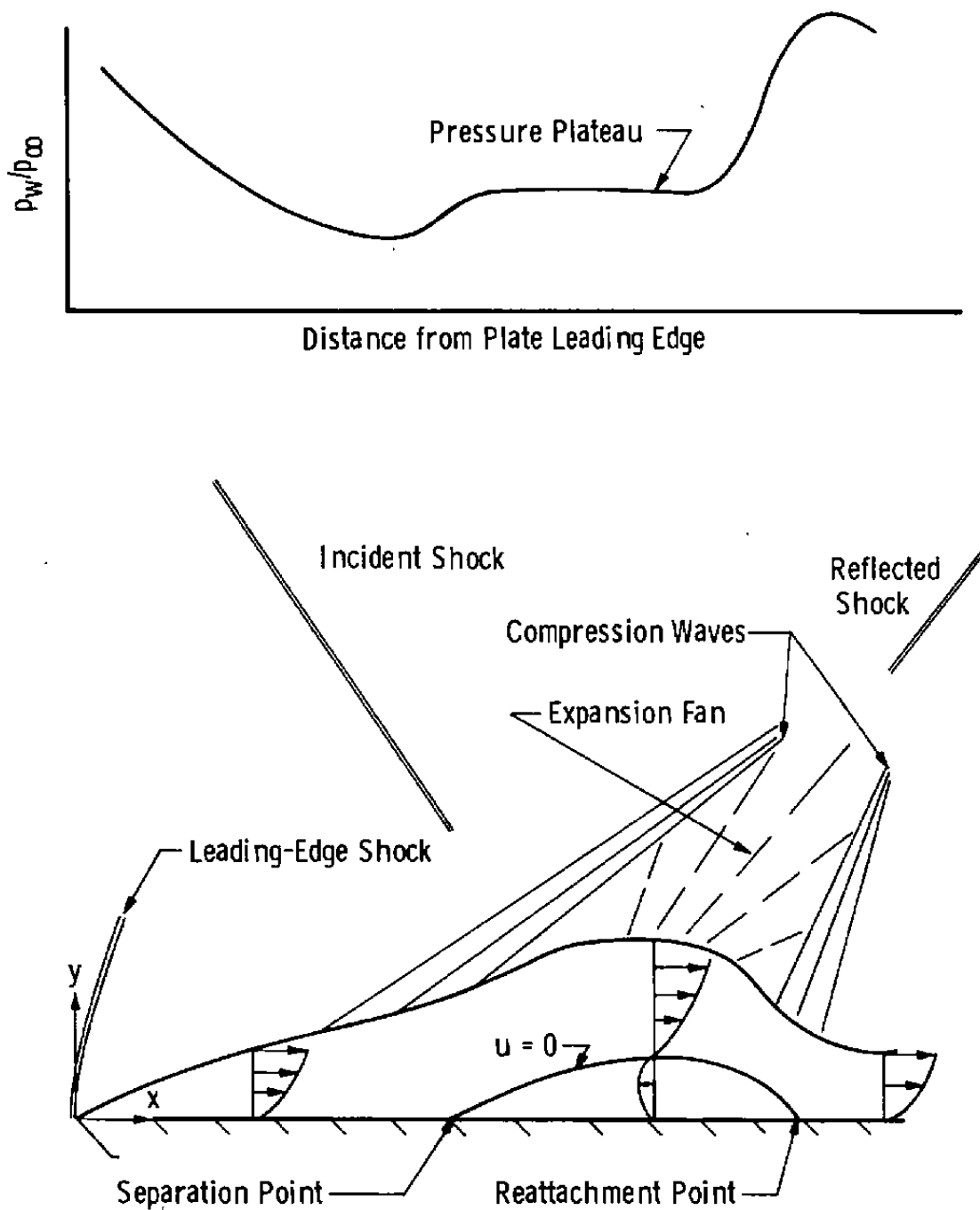
Figure 1. Schematic of boundary -layer/shock—wave interaction.

Stokes equations, from which the Euler equations and the boundary-layer equations are derived, are fundamental to the subject of viscous fluid flow and are valid throughout the entire flow field. The Navier-Stokes equations will yield valid results at separation and reattachment, within the separated recirculation region, across incident and reflected shock waves, throughout expansion fans, and for any combinative influences of the aforementioned. The equations require numerical solution in either a spatially elliptic or a temporally hyperbolic domain.

The present report compares numerical results from an explicit time-dependent compressible Navier-Stokes analysis developed by MacCormack (Ref. 1) with experimental data for hypersonic laminar boundary-layer/shock-wave interaction on a flat plate under AEDC von Kármán Gas Dynamics Facility (VKF), Hypersonic Wind Tunnel (B), conditions as well as NASA Langley Research Center (LRC) Mach 8 Variable Density Tunnel conditions. It is shown that numerical solutions of the time-dependent compressible Navier-Stokes equations yield reasonable results when applied to hypersonic laminar boundary-layer/shock-wave interactions.

## 2.0 ANALYTICAL ANALYSIS

## 2.1 TIME–DEPENDENT METHOD OF SOLUTION OVERVIEW

The time-dependent method starts with a complete specification of the flow field and then uses the governing equations of motion to advance the flow field temporally until a steady state is reached. Thus, the flow field evolves numerically in a process analogous with physical reality. The initial specification can be just a uniform flow with appropriate boundary conditions (see Roache (Ref. 2) and Richtmyer and Morton (Ref. 3) for general expositions on the time-dependent method).

The physical basis of the time-dependent approach as well as the advantages accrued by application of the time-dependent method to solve the compressible Navier-Stokes equations were delineated by Crocco in 1965 (Ref. 4). Kurzrock and Mates (Ref. 5) in 1966 used the time-dependent approach to study analytically the flow in a shock tube and hypersonic flow over a sharp flat plate. Skoglund and Gay (Ref. 6) applied the time-dependent method to the computation of laminar boundary-layer/shock-wave interactions in 1969.

## 2.2 THE EXPLICIT TIME—DEPENDENT METHOD OF MACCORMACK

The so-called method of MacCormack, since its introduction in 1969, has become one of the most widely used explicit second-order accurate methods for numerical solution of hyperbolic partial differential equations. The algorithm was first introduced by MacCormack in Ref. 7 and subsequently modified and extended by Refs. 8 through 14 as well as Ref. 1. It has been applied to obtain solutions of the time-dependent compressible Navier-Stokes equations by Baldwin and MacCormack (Refs. 9 and 10), MacCormack and Baldwin (Ref. 11), and Deiwert (Refs. 15 and 16) among others.

The two-dimensional time-dependent Navier-Stokes equations, neglecting body forces and heat generation, can be written in conservation form as:

$$\frac{\partial U}{\partial t} + \frac{\partial F}{\partial x} + \frac{\partial G}{\partial y} = 0 \qquad (1)$$

where

$$U = \begin{bmatrix} \rho \\ \rho u \\ \rho v \\ e \end{bmatrix} \qquad (2)$$

$$F = \begin{bmatrix} \rho u \\ \rho u^2 + \sigma_x \\ \rho uv + \tau_{xy} \\ (e + \sigma_x)u + \tau_{yx}v - k\partial T/\partial x \end{bmatrix} \tag{3}$$

$$G = \begin{bmatrix} \rho v \\ \rho uv + \tau_{yx} \\ \rho v^2 + \sigma_y \\ (e + \sigma_y)v + \tau_{xy}u - k\,\partial T/\partial y \end{bmatrix} \tag{4}$$

with

$$\sigma_x = p - \lambda\left(\frac{\partial u}{\partial x} + \frac{\partial v}{\partial y}\right) - 2\mu\frac{\partial u}{\partial x} \tag{5}$$

$$\tau_{xy} = \tau_{yx} = -\mu\left(\frac{\partial u}{\partial y} + \frac{\partial v}{\partial x}\right) \tag{6}$$

$$\sigma_y = p - \lambda\left(\frac{\partial u}{\partial x} + \frac{\partial v}{\partial y}\right) - 2\mu\frac{\partial v}{\partial y} \tag{7}$$

(see the Nomenclature for terminology).

The procedure used to advance the dependent variables ($\rho$, $\rho u$, $\rho v$, e) from a time t to a time t + $\Delta$t at the interior points will be examined first. The procedures for the boundary points are different and will be reviewed subsequently. The MacCormack method is of the predictor-corrector type and can be utilized in such a manner that a single predictor and a single corrector application will advance the dependent variables in time by an amount $\Delta$t. However, if the concept of splitting is employed, simplicity and computational efficiency result (Ref. 8). Basically the concept of splitting involves a predictor-corrector pass driven by gradients in the x-direction and a separate predictor-corrector pass driven by gradients in the y-direction. Thus four sweeps, two predictor and two corrector, are required. This may be written as:

9

$$\overline{U_{i,j}^{n+1/2}} = U_{i,j}^{n} - \left(\frac{\Delta t}{\Delta y}\right)\left(G_{i,j}^{n} - G_{i,j-1}^{n}\right) \tag{8}$$

$$U_{i,j}^{n+1/2} = \frac{1}{2}\left(U_{i,j}^{n} + \overline{U_{i,j}^{n+1/2}}\right) - \frac{1}{2}\left(\frac{\Delta t}{\Delta y}\right)\left(\overline{G_{i,j+1}^{n+1/2}} - \overline{G_{i,j}^{n+1/2}}\right) \tag{9}$$

and

$$\overline{U_{i,j}^{n+1}} = U_{i,j}^{n+1/2} - \left(\frac{\Delta t}{\Delta x}\right)\left(F_{i,j}^{n+1/2} - F_{i-1,j}^{n+1/2}\right) \tag{10}$$

$$U_{i,j}^{n+1} = \frac{1}{2}\left(U_{i,j}^{n+1/2} + \overline{U_{i,j}^{n+1}}\right) - \frac{1}{2}\left(\frac{\Delta t}{\Delta x}\right)\left(\overline{F_{i+1,j}^{n+1}} - \overline{F_{i,j}^{n+1}}\right) \tag{11}$$

Denoting by Lx the operation performed by Eqs. (8) and (9) and by Ly the operation performed by Eqs. (10) and (11), the sequence becomes

$$U^{n+1} = LxLyU^{n} \tag{12}$$

This operation (Eq. (12)) is not of second-order accuracy but

$$U^{n+1} = Ly\left(\frac{\Delta t}{2}\right) Lx\left(\frac{\Delta t}{2}\right) Lx\left(\frac{\Delta t}{2}\right) Ly\left(\frac{\Delta t}{2}\right) U^{n} \tag{13}$$

retains second-order accuracy. The stability criterion (the Courant-Friedrichs-Lewy condition) for the y sweep is:

$$\Delta t_y = \frac{\Delta y}{|v| + c} \tag{14}$$

and for the x-sweep

$$\Delta t_x = \frac{\Delta x}{|u| + c} \tag{15}$$

The minimum of Eqs. (14) and (15) for the entire grid represents the maximum $\Delta t$ for which computational stability is ensured. The sequence of operations defined by Eq. (13) is used to advance temporally the interior points of the computational grid. The boundary condition treatment and the initial condition specifications are needed to complete the method.

The numerical solution of flows containing strong shock waves is often hampered by numerical oscillations which can eventually cause program failure. A fourth-order damping term, effective only in regions of large pressure gradients, has been used to reduce the numerical oscillations (Refs. 9, 10, and 11). Essentially, this technique adds an additional "viscosity" proportional to the second derivative of pressure to each of the steps represented by Eqs. (8) through (11). The addition in regions of low-pressure gradients is negligible and is of importance only where pressure gradients or pressure oscillations are large. By using the arrow symbol to denote replacement, the damping terms can be included in Eqs. (8) through (11) by

$$G_{i,j}^n \leftarrow G_{i,j}^n + \Delta G_{i,j}^n \qquad (16)$$

$$F_{i,j}^{n+1/2} \leftarrow F_{i,j}^{n+1/2} + \Delta F_{i,j}^{n+1/2} \qquad (17)$$

where

$$\Delta G_{i,j}^n = \frac{1}{2}(|v| + c)_{i,j} \frac{P_{i,j+1} - 2\,P_{i,j} + P_{i,j-1}}{P_{i,j+1} + 2\,P_{i,j} + P_{i,j-1}} (U_{i,j+1} - U_{i,j}) \qquad (18)$$

$$\Delta F_{i,j}^{n+1/2} = \frac{1}{2}(|u| + c)_{i,j} \frac{P_{i+1,j} - 2\,P_{i,j} - P_{i-1,j}}{P_{i+1,j} + 2\,P_{i,j} + P_{i-1,j}} (U_{i+1,j} - U_{i,j}) \qquad (19)$$

The quantities $G_{i,j-1}^n$ and $F_{i-1,j}^{n+1/2}$ are treated in the same manner as indicated in Eqs. (16) through (19) as are all the barred quantities; i.e., to each F or G term in Eqs. (8) through (11) is added the term analogus to Eq. (18) or (19).

## 2.3 INITIAL AND BOUNDARY CONDITIONS

Initially, the flow field must be specified completely in the region under consideration, the computational plane. The computational plane for the boundary-layer/shock-wave interaction is shown schematically in Fig. 2. All of the flow field except the upper boundary (line AB in Fig. 2) need be specified only as a uniform flow. The upper boundary is specified in such a manner that the incident shock impacts the surface at the desired location. By specifying uniform flow along line AE and Rankine-Hugoniot flow conditions along line EB, such can be accomplished. The boundary layer will form normally on the surface, the shock will spread downward, and the interaction will evolve in the correct manner.
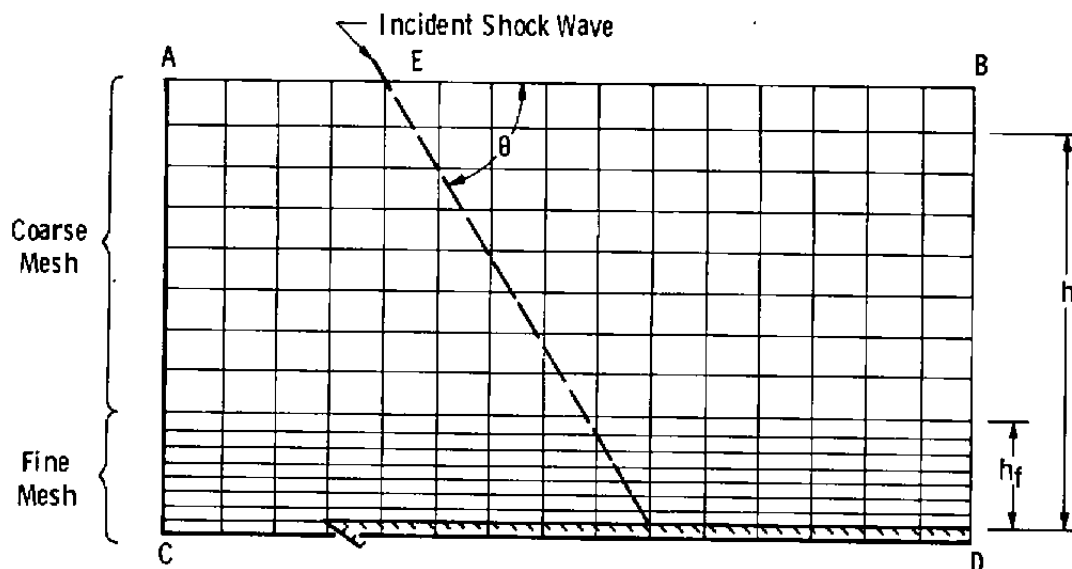
Figure 2. Computational mesh system for boundary—layer/shock—wave interaction.

As the solution advances, only the boundary conditions along AB, AC, and CD must be specified. Along AEB, the same conditions initially specified must be used. Segment BD cannot be defined as this would overspecify the problem. A gradient condition such as $\partial/\partial x = 0$ along BD is used since a large portion of the flow field is supersonic and will thus not propogate errors upstream. This specification of region

BD does not introduce spurious information into the remainder of the flow field. Region AC can be taken as a uniform flow field if the leading edge of the plate is to be considered or input as previously determined profiles if the area of interest is too large for normal processing. Both input profiles and input uniform flow have been used with good results. The wall boundary conditions are defined along CD in such a manner that flat plate results are obtained midway between the first two grid rows; i.e.,

$$u_{i,1} = -u_{i,2} \tag{20}$$

$$v_{i,1} = -v_{i,2} \tag{21}$$

$$e_{i,1} = C_v(2T_w - e_{i,2}/C_v) \tag{22}$$

$$P_{i,1} = P_{i,2} - \Delta y \left(\frac{\partial p}{\partial y}\right)_{i,2} \tag{23}$$

$$\rho_{i,1} = \frac{P_{i,1}}{(\gamma - 1)e_{i,1}} \tag{24}$$

## 2.4 COMPUTATIONAL GRID

Some consideration on the nature of the expected solution is relevant at this point. The flow field may be viewed as being composed of an outer region basically inviscid in nature and an inner viscous-dominated region. The outer region will change only gradually as the interaction evolves; and, therefore, will need to be computed less frequently. Since the maximum allowable time step in an explicit time-dependent method is proportional to the grid spacing (as indicated by Eqs. (14) and (15)), the finer the grid the smaller the allowable time step $\Delta t$. If a fine grid is used in the viscous-dominated region and a coarse grid is used in the outer inviscid-like region, computations will need to be performed in the coarse-grid region only once for every M times in the fine-grid region. M is the smallest integer plus one in the quotient of the smallest $\Delta t$ in the coarse grid and the smallest $\Delta t$ in the fine grid, i.e.,

$$M = MOD(\Delta t_c, \Delta t_f) + 1 \tag{25}$$

Figure 2 illustrates the computational grid used, showing the fine and coarse regions. Thus, most of the computational effort will be expended in the viscous-dominated region. Caution must be exercised at the boundary between the fine and coarse grids as accumulation or origination of conserved quantities can introduce computational anomalies to the solution.

The basic digital computer code follows the University of Tennessee Space Institute Short Course notes as given by MacCormack (Ref. 17). All numerical results reported herein were generated using an IBM 370/165 digital computer. The computer program was executed using single precision arithmetic and required 372,000 bytes of core for a 183 by 35 grid array using the IBM FORTRAN IV H-LEVEL 21.7 Compiler. Typically about 100 sec of CPU time were required for one complete pass through the program (advancement of the field from time t to time t + Δt) for a 183 by 35 array. The code was modified to have restart capability and to permit various initial-condition options to be exercised.

## 3.0 RESULTS

The von Kármán Facility at AEDC is concerned primarily with high supersonic and hypersonic flows. Since only boundary-layer/shock-wave interactions that are completely laminar are examined in this report, relatively low-incident shock-wave angles are required at the hypersonic Mach numbers of interest. Large-incident shock-wave angles at hypersonic Mach numbers and the corresponding large pressure increases across the incident/reflected shock-wave systems preclude the maintenance of laminar flows throughout the interaction region. Laminar interactions were considered since it was deemed desirable to validate the explicit time-dependent method for numerically solving the Navier-Stokes equations prior to any considerations of the complicating effects of turbulent flow. Attempts at turbulent boundary-layer/shock-wave interaction solutions by Baldwin and MacCormack (Refs. 9 and 10) and by Horstman,

et al. (Ref. 18), indicate that much development is needed in turbulence modeling before transitional and turbulent processes can be adequately treated.

## 3.1 BOUNDARY—LAYER/SHOCK—WAVE INTERACTIONS

Prior to discussing numerical solutions, it is appropriate to examine typical wind tunnel models and inviscid solutions for shock reflection. Figure 3 (taken from the study reported in Ref. 19) shows typical VKF Tunnel B apparatus used to investigate boundary-layer/shock-wave interactions. The upper wedge (generator) produces an oblique shock wave that impinges on the lower wedge (receiver). Impingement location as well as shock strength can be easily controlled using such an arrangement. Pressure or heat-transfer data are taken from the receiver plate. Because of viscous-induced effects near the leading edge of the generator, the oblique shock angle produced is not the "wedge" shock angle that the nominal generator angle of attack would produce. The receiver plate leading edge also exhibits viscous-induced effects, one obvious result being the leading-edge shock. The aforementioned effects are such that, for nominal given angles, the inviscid pressure ratios across the incident/reflected shock waves are not obtained.

Numerical solutions corresponding to particular experimental cases have been generated by using the experimental ratio $p_3/p_1$ (see Sketch 1) and the free-stream Mach number ($M_\infty$) to define the inviscid shock angle ($\theta$). This allowed the correct pressure ratio to be used
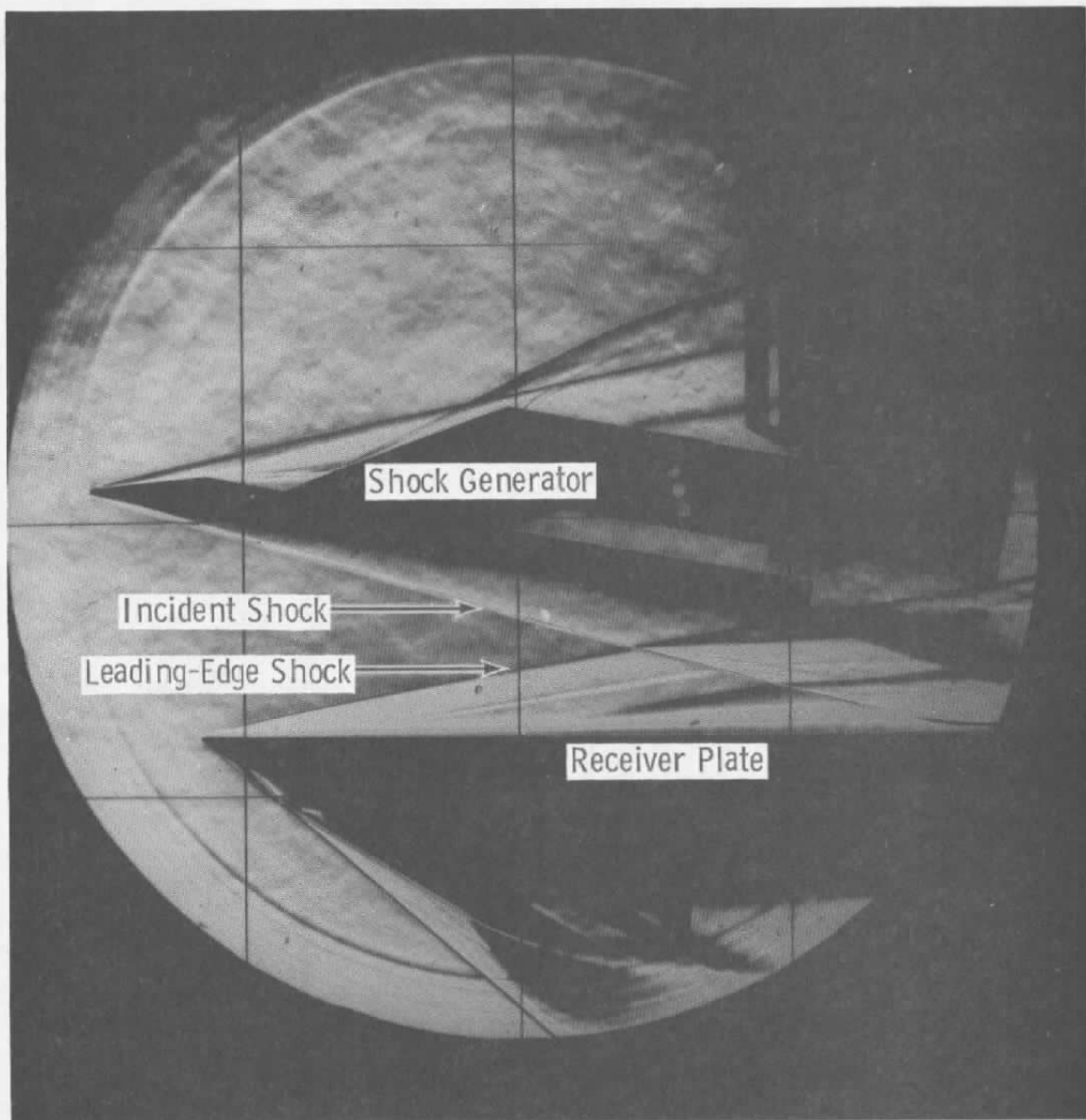


Sketch 1
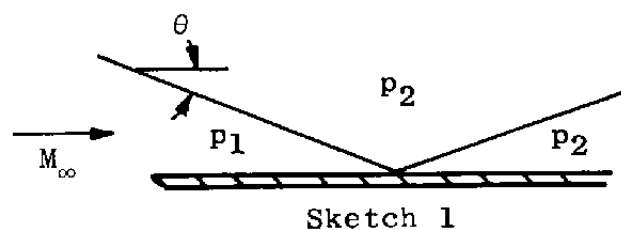
Figure 3. Schlieren photograph of shock generator and
receiver plate in AEDC Tunnel B (taken from
the study reported in Ref. 19).

without expending additional computational effort to define viscous-induced effects on the generator. Figure 4 was computed using inviscid-flow wedge results and allows the rapid estimate of the appropriate incident shock angle ($\theta$) for a given free-stream Mach number and pressure ratio. Additionally, the minimum and maximum incident shock angle for a normal reflection is given. It is interesting to note that, for a diatomic gas ($\gamma = 1.4$) and free-stream Mach number greater than about 3, a regular reflection is not admissible for a shock angle greater than 40 deg. A more detailed examination was given by Zumwalt (Ref. 20).

Figure 5 (taken from the study reported in Ref. 19) is a schlieren photograph of a typical laminar boundary-layer/shock-wave interaction. The incident/reflected shock-wave system can be seen. The dashed lines indicate the nominal region used in the computation. However, for a region which does not contain the leading edge of the plate, suitable profiles in density, velocity, energy, and pressure must be available for use as initial and boundary conditions for the upstream (left-hand side in Fig. 5) computational boundary. The required profiles could have been generated by a typical parabolic boundary-layer program, but the viscous-induced leading edge effects prominent in hypersonic flow (see Fig. 3) would not have been present. Since a compressible Navier-Stokes solution is capable of generating such effects, the computer code without an incident shock wave possessed the capability of calculating laminar flat-plate profiles including viscous-induced leading-edge effects. Thus, whenever it was desired to start an interaction computation without including the plate leading edge, a suitable set of initial profiles was obtained by generating a flat-plate Navier-Stokes solution including the leading edge and retaining the required numerical information on a data storage device. Baldwin and MacCormack (Ref. 9) used this technique in their turbulent boundary-layer/shock-wave calculations as did Carter (Ref. 21) in his laminar calculations on a supersonic ramp.
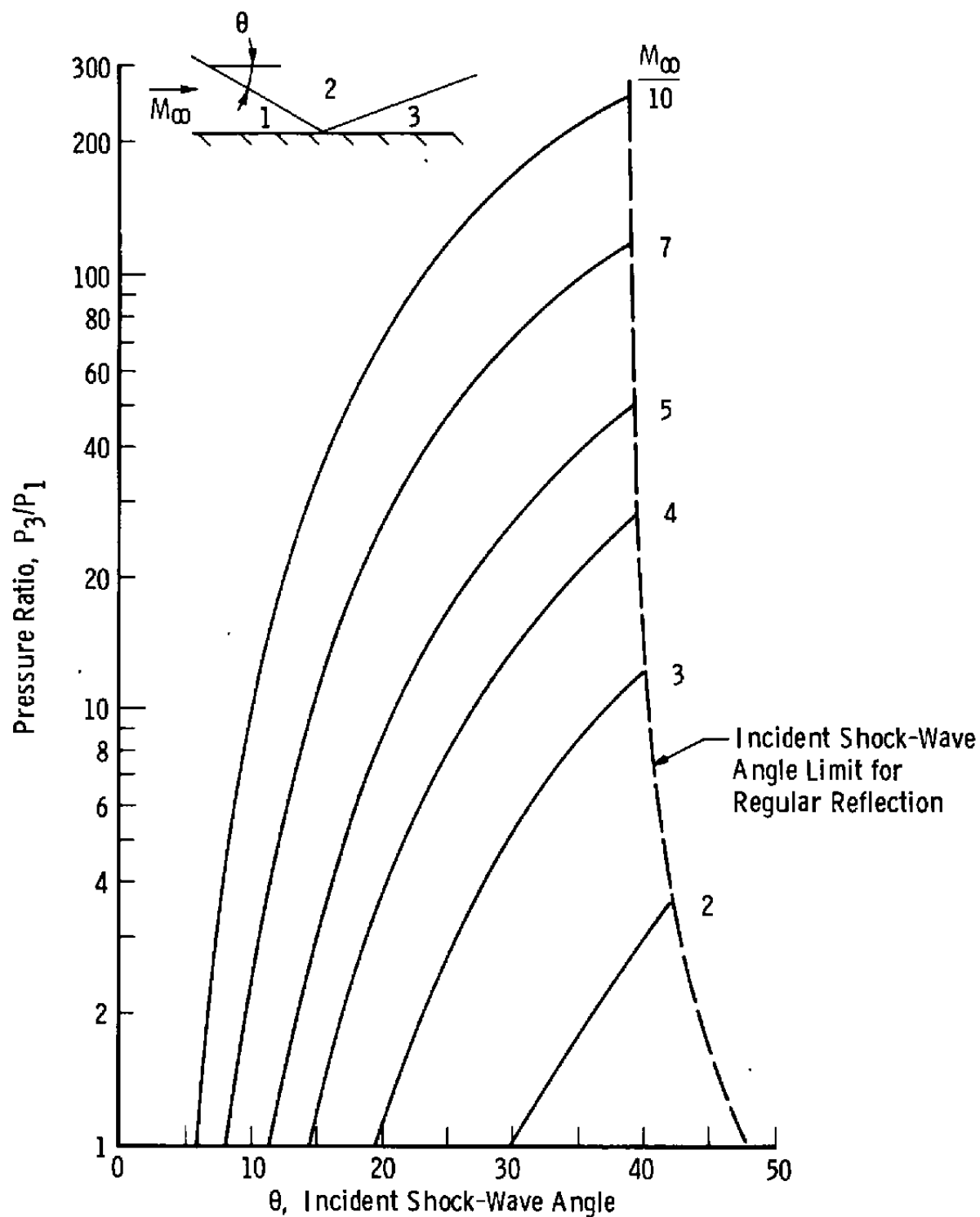
Figure 4. Inviscid pressure ratios for incident—reflected shock wave.
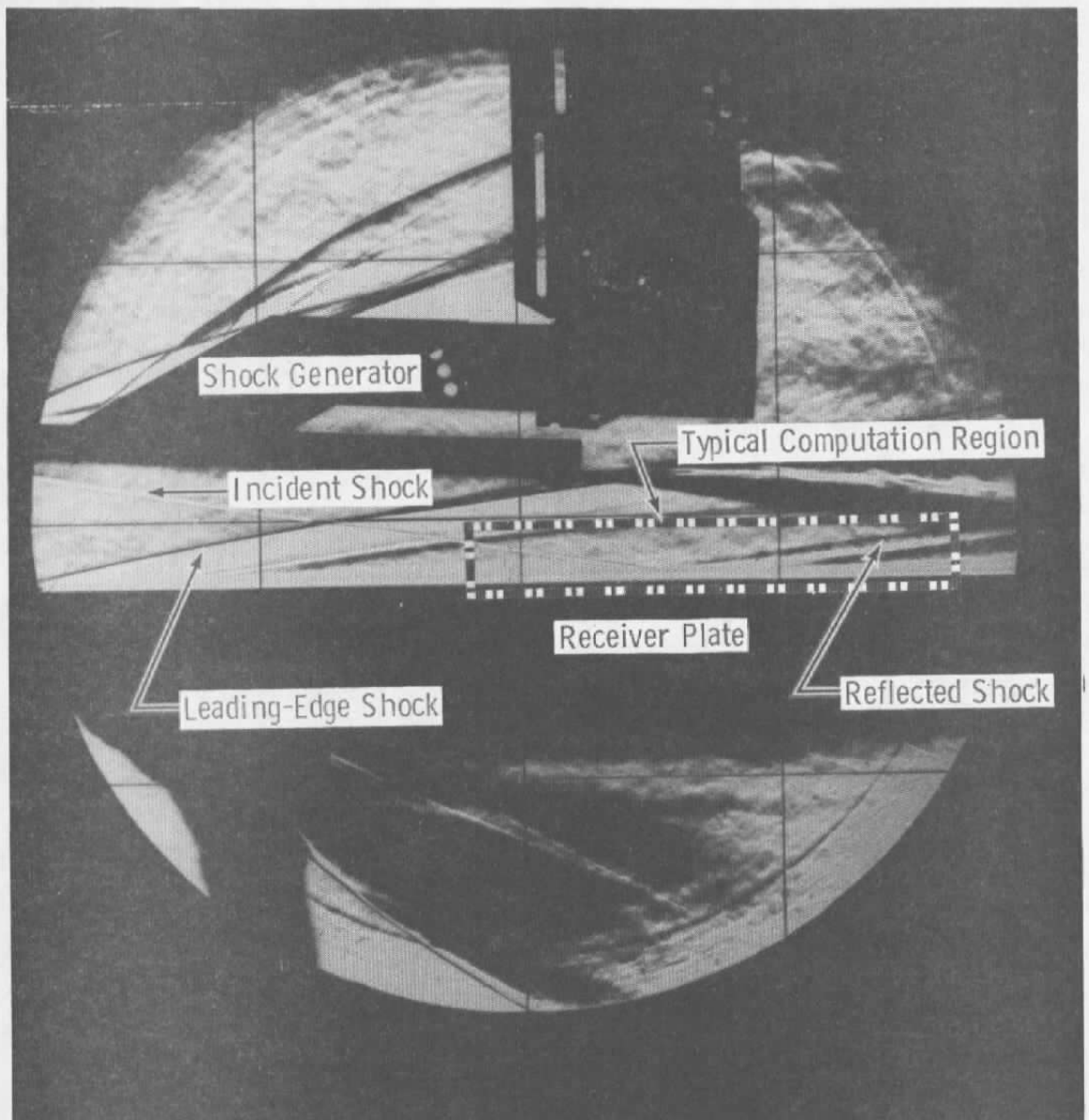
Figure 5.  Schlieren photograph of a boundary—layer/shock—wave
interaction in AEDC Tunnel B (taken from the study
reported in Ref. 19).

## 3.2  NUMERICAL RESULTS

As a check on the capability of the code, a low Reynolds number flat-plate solution was generated using the conditions of Carter (Ref. 21). The resulting pressure distribution is shown in Fig. 6 along with the time-dependent compressible Navier-Stokes numerical solution of Carter. Both solutions exhibit essentially the same behavior except very close to the leading edge where the explicit MacCormack scheme is smoother than the Brailovskaya scheme used by Carter.
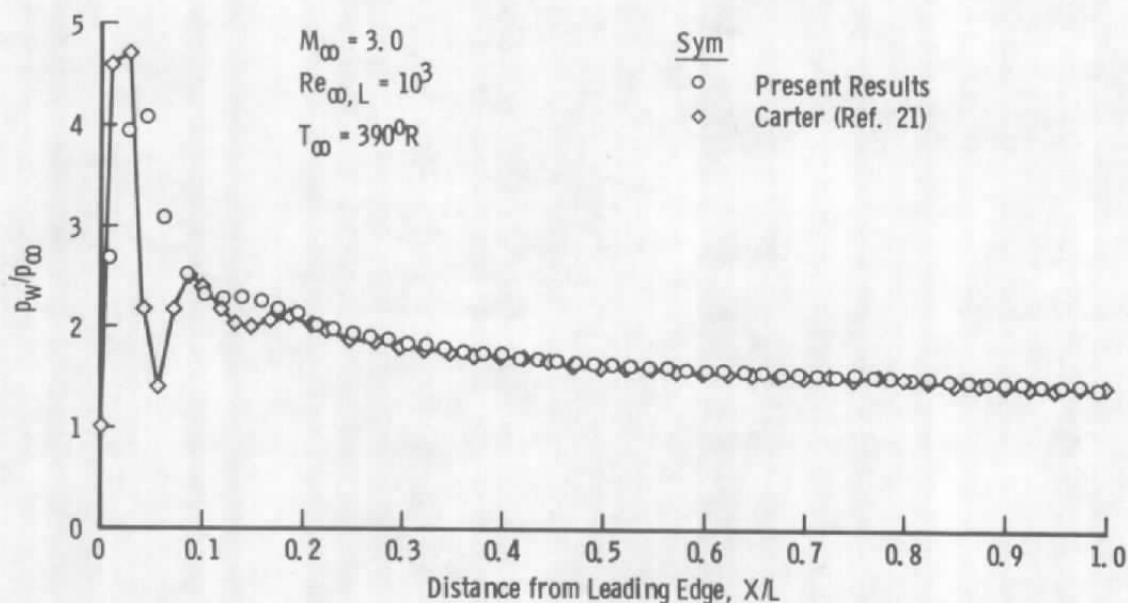


Figure 6.  Flat plate pressure distributions computed by the MacCormack Algorithm and the Brailovskaya Algorithm.

Depending on the state of the boundary layer and the magnitude of the pressure jump across the incident/reflected shock-wave system, flow separation and reattachment with a recirculation region may occur.  This condition is schematically illustrated in Fig. 1.  The presence of a separation region with recirculation and reattachment poses a more severe test of the code's capability than an unseparated case.  Thus, to avoid possible complications resulting from separated regions, the

first results examined will be for non-separated hypersonic flows. All the numerical results reported herein were obtained using a constant wall temperature for the receiver plate. Data which would allow a more exact specification of wall temperature were not generally available.

All of the VKF Tunnel B data examined in the present study had the nominal shock interaction point one foot from the leading edge of the plate. The parameters used in the numerical solution are given in Table 1, which contains tabular information for all the cases examined. The first laminar boundary-layer/shock-wave interaction presented (number 2 of Table 1) was generated using a set of profiles (density, velocity, internal energy) computed via the time-dependent compressible Navier-Stokes code with no impinging shock wave. Figure 7 is a partial reproduction of the input velocity ratio profiles ($u/U_\infty$) generated and is typical of the profiles. Figure 8 shows the computed streamline shapes for the leading edge of the flat plate, and Fig. 9 shows the shape of the leading-edge shock. Shock-wave locations in the "shock-capturing" MacCormack code were estimated by computing the first and second derivatives of pressure with respect to longitudinal distance and locating regions where $dp/dx$ is a maximum and $d^2p/dx^2$ is large. This is similar to the philosophy of Grossman and Moretti (Ref. 22) in locating incipient shock waves in inviscid time-dependent calculations.

By using the aforementioned input profiles and a shock-wave angle of 8.6 deg, a boundary-layer/shock-wave interaction was generated. This corresponded to conditions for which VKF Tunnel B data were available (Ref. 19). Figure 10 presents the results of the computed interactions as well as the VKF Tunnel B data for the corresponding tunnel conditions. Agreement is satisfactory particularly near the peak pressure location where the correct shape is generated and in the mid-range where the correct pressure gradient is obtained. No evidence of separation was obvious from the data, and no separated region was predicted by the program. Because of the rather modest

pressure rise across the incident/reflected shock-wave system and because of the lack of separation, it is probable that this is a completely laminar interaction. Overall agreement with the laminar time-dependent Navier-Stokes solution tends to confirm this. Computer time on an IBM 370/165 was 2 hr for the flat-plate solution from which the initial profiles were secured and 3 hr for the interaction.

Table 1. Parameters for Numerical Cases

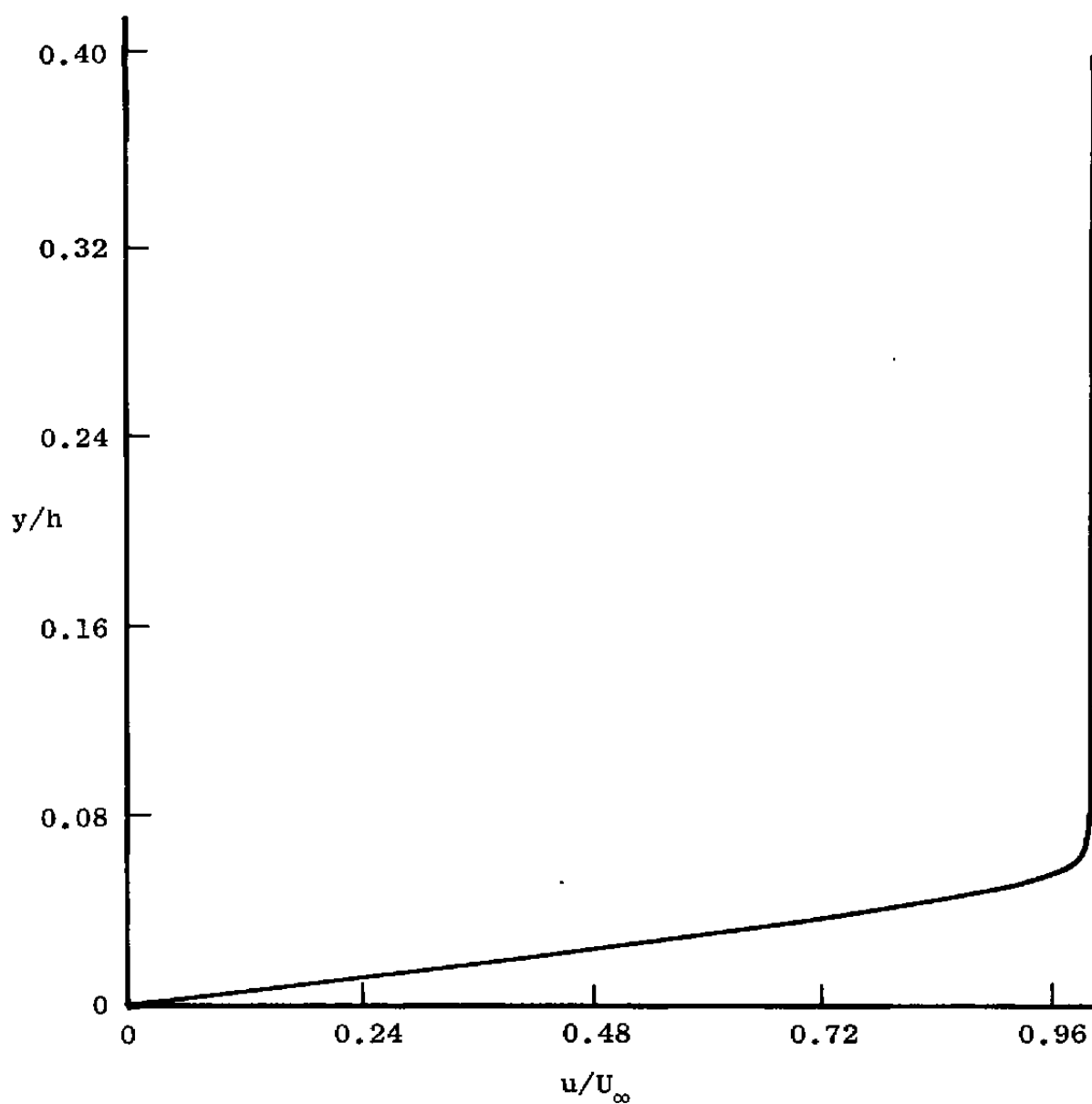| No. | Tunnel | $M_\infty$ | $Re_\infty/ft$ | $T_\infty,$ $^\circ R$ | $p_\infty,$ $lb/ft^2$ | $T_w,$ $^\circ R$ | $h_f,$ ft | $h,$ ft | $\theta,$ deg | IMAX | JMAX |
|---|---|---|---|---|---|---|---|---|---|---|---|
| 1 | VKF B | 7.94 | $0.96 \times 10^6$ | 93.68 | 2.885 | 520.0 | 0.035 | 0.35 | --- | 46 | 40 |
| 2 | VKF B | 7.94 | $0.96 \times 10^6$ | 93.68 | 2.885 | 520.0 | 0.035 | 0.35 | 8.6 | 66 | 40 |
| 3 | NASA LRC Mach 8 | 7.73 | $0.48 \times 10^6$ | 100.6 | 2.120 | 530.4 | 0.035 | 0.35 | 11.1 | 60 | 40 |
| 4 | VKF B | 7.93 | $0.97 \times 10^6$ | 94.43 | 3.140 | 525.0 | 0.030 | 0.25 | 10.7 | 171 | 25 |
| 5 | VKF B | 7.94 | $0.96 \times 10^6$ | 93.68 | 2.885 | 520.0 | 0.035 | 0.35 | 16.0 | 181 | 35 |

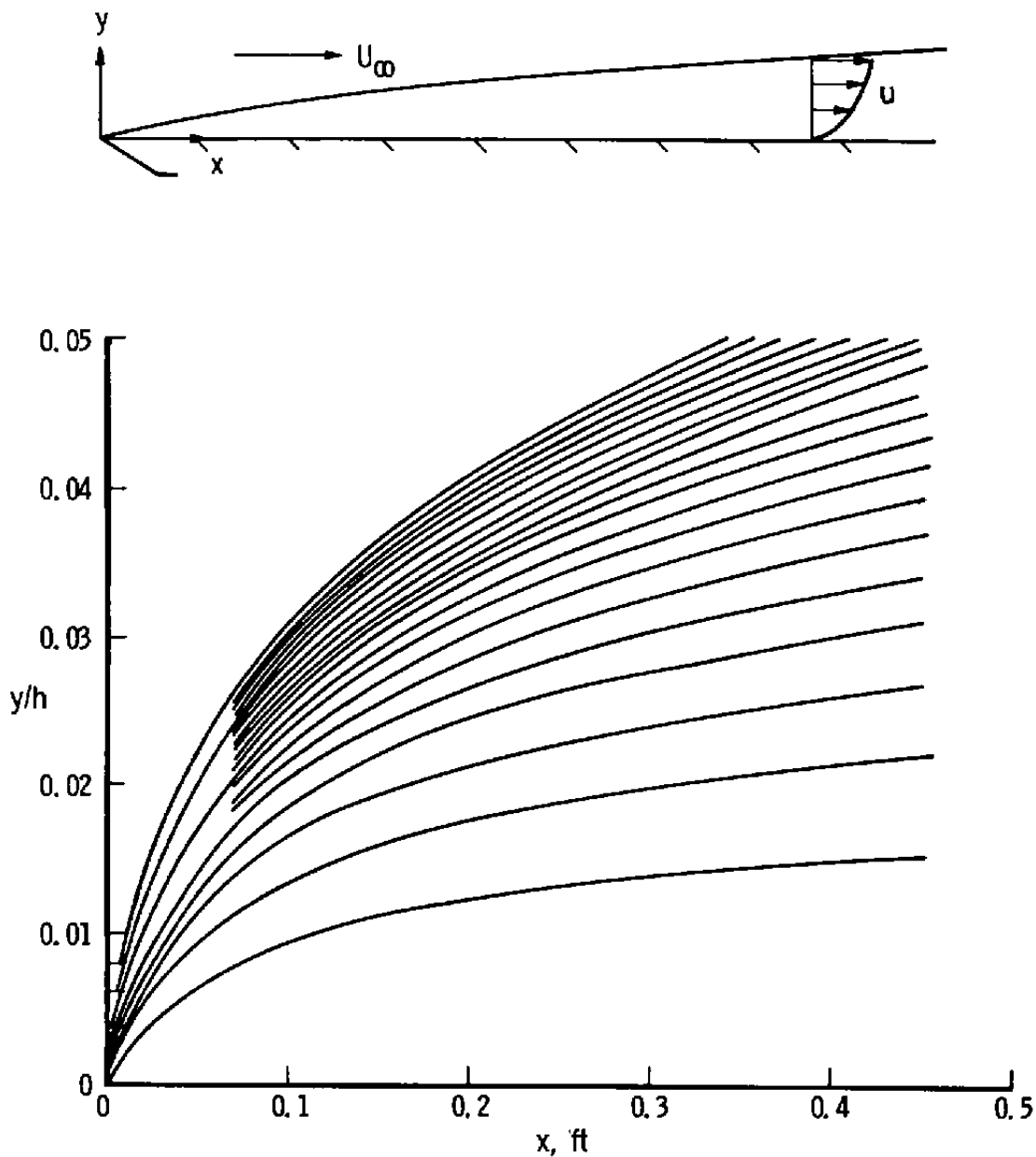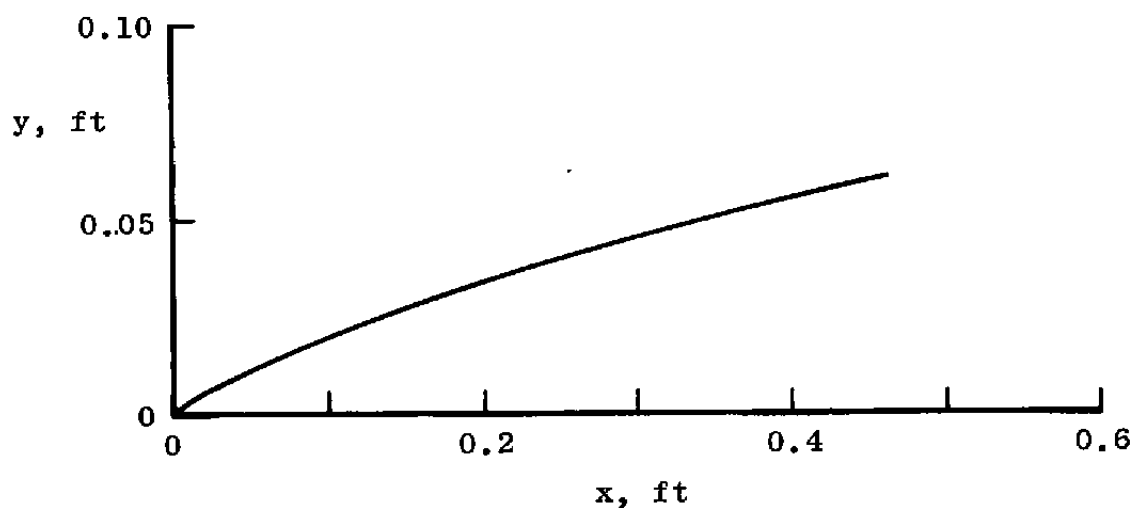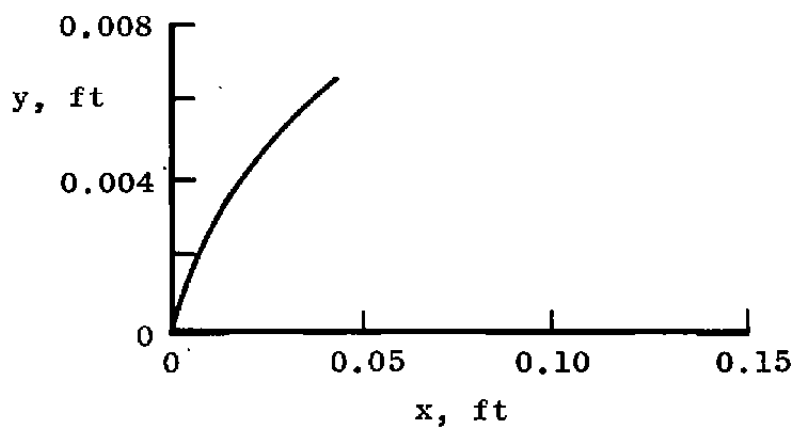Figure 7.  Flat plate velocity profile.

Figure 8. Streamlines near the leading edge of a flat plate at hypersonic velocities.

a. Shock wave shape



b. Leading edge detail

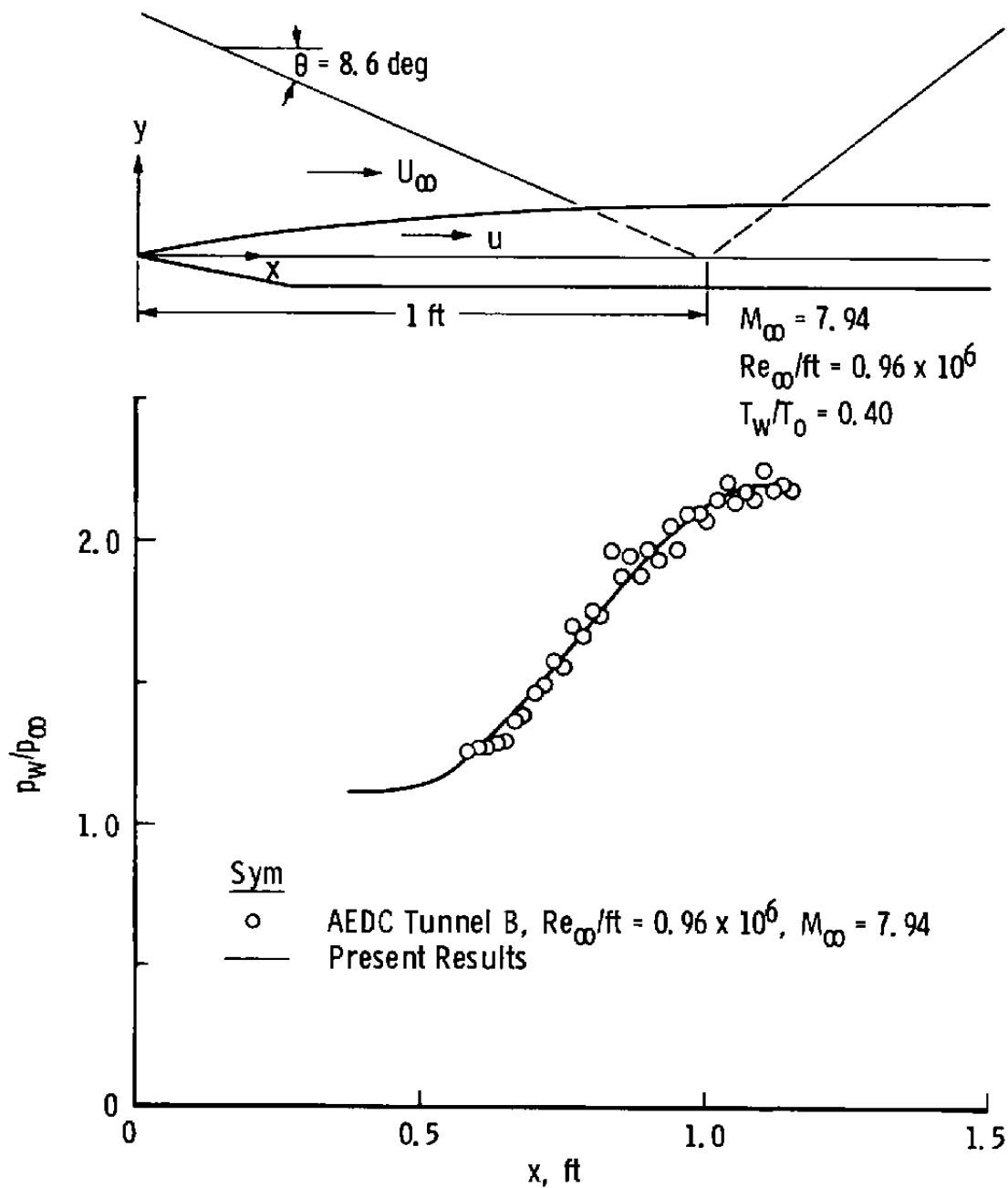Figure 9. Leading edge shock shape for a flat plate at hypersonic velocities.

Figure 10. Laminar hypersonic boundary—layer/shock—wave interaction using VKF Tunnel B conditions.

An additional hypersonic laminar boundary-layer/shock-wave interaction using as a basis the data of Kaufman and Johnson (Ref. 23) taken in the Langley Research Center (LRC) Mach 8 Variable Density Tunnel was attempted. The results of the computation as well as the relevant experimental data are presented in Fig. 11. Agreement is satisfactory particularly near the peak pressure location. The predicted pressure gradient within the interaction region agrees well with the experimental data. The major discrepancy occurs near the beginning of the interaction region where the experimental pressure is about 50 percent higher than the computed pressure. It is tempting to ascribe the anomaly to viscous-induced phenomena from the leading edge of the plate, but the results of Fig. 6 give some confidence in the ability of the code to properly compute viscous-induced effects. Local variations in wall temperature as well as the overall model temperature can affect the pressure in the vicinity of the leading edge. Kaufman and Johnson suggest using a uniform model temperature of 0.5 times the total temperature. This suggestion was followed in making the computations and could have contributed to the discrepancy as the exact model temperature distribution was not known. Six hours of IBM 370/165 CPU time were required.

Heat transfer is another of the quantities commonly measured in experiments and needed from calculations. Thus, the capability of the code to predict the level of heat transfer in a laminar boundary-layer/shock-wave interaction is also of interest. Figure 12 was generated using as a basis heat-transfer data from the VKF Tunnel B (Ref. 18). The agreement between the computed free-stream Stanton number ($St_\infty$) and the measured free-stream Stanton number is disappointing. The computed solution underpredicts the maximum heating rate and overpredicts the minimum heating rate. The numerical solution indicates no separation to be present, and an examination of the data indicates little, if any, separation. Thus, the problem appears to be one of grid resolution as qualitatively the correct trends are observed in the computer-generated solution.

27

$\theta = 11.1$ deg

$M_\infty = 7.73$

$Re_\infty/ft = 0.481 \times 10^6$

$T_w/T_0 = 0.5$

0.889 ft

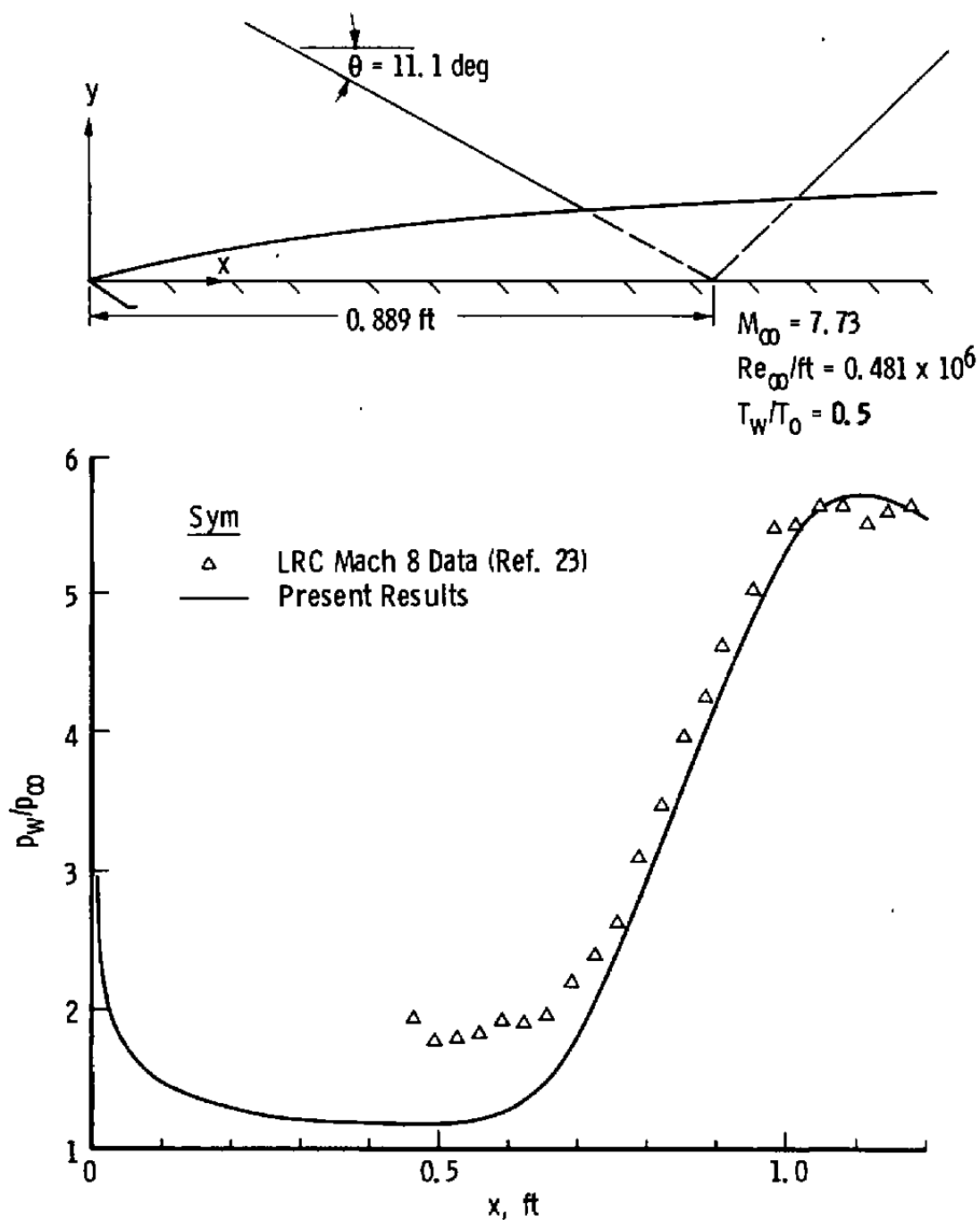| Sym | |
|---|---|
| $\triangle$ | LRC Mach 8 Data (Ref. 23) |
| —— | Present Results |

Figure 11. Laminar hypersonic boundary—layer/shock—wave interaction using LRC Mach 8 tunnel conditions.
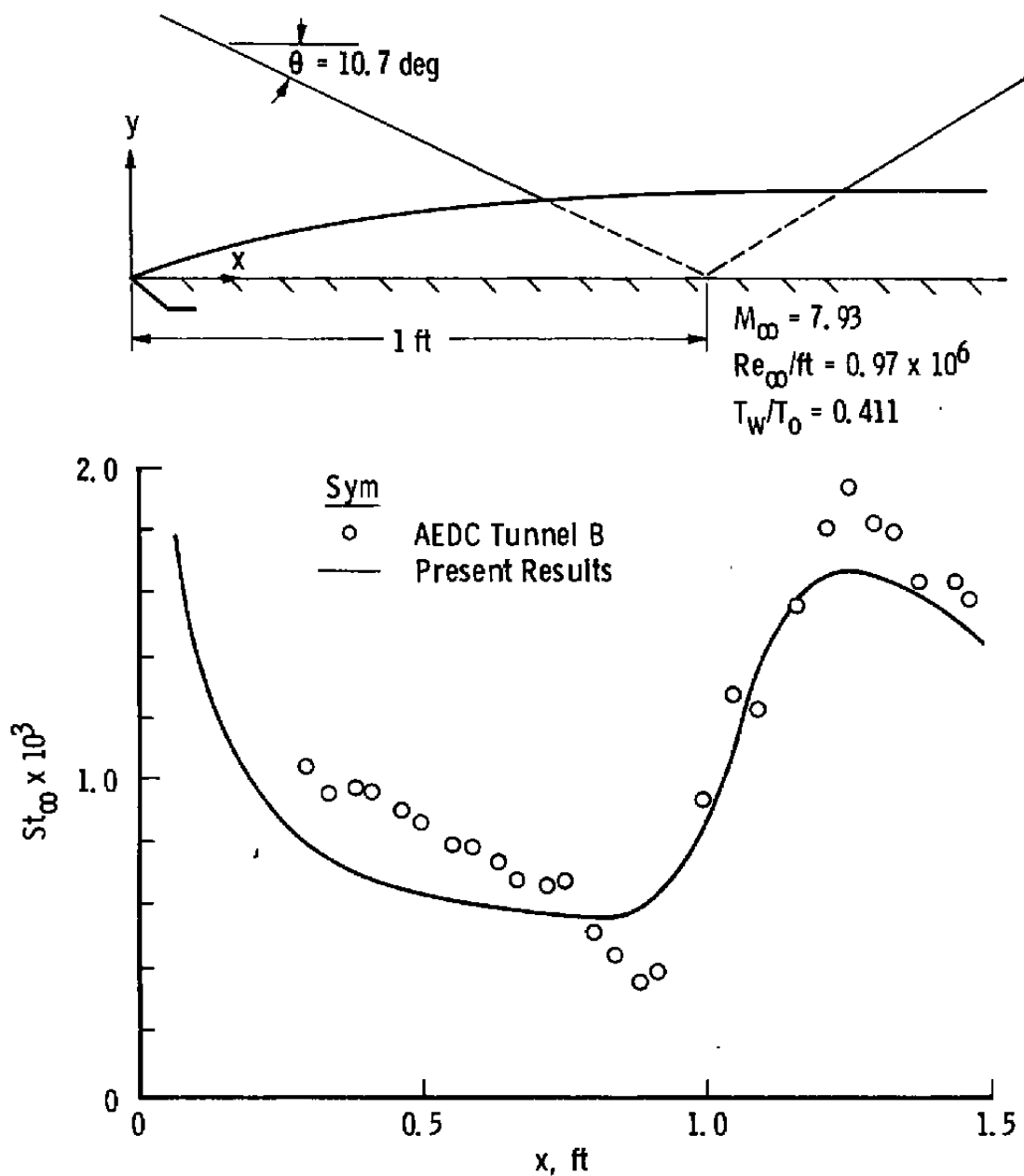
Figure 12. Heat transfer for a laminar hypersonic boundary—layer/shock—wave interaction using VKF Tunnel B conditions.

The cell Reynolds number as an index of spatial resolution has previously been examined by Roache (Ref. 2), Cheng (Ref. 24), and MacCormack (Ref. 11). MacCormack, for example, suggests a cell Reynolds number on the order of two for each coordinate mesh spacing if every term of the Navier-Stokes equations is to receive adequate support. For this particular case, a cell Reynolds number based on $\Delta y$ within the viscous-dominated region has a typical value of 6.0; i.e.,

$$Re_{\Delta y} = \frac{\rho v \Delta y}{\mu} \approx 6.0 \tag{26}$$

and the cell Reynolds number based on $\Delta x$ within the viscous-dominated region has a typical value of 1,250; i.e.,

$$Re_{\Delta x} = \frac{\rho u \Delta x}{\mu} \approx 1,250 \tag{27}$$

Thus, the y-mesh should adequately support all terms, while the x-mesh will not adequately support all terms. Obviously, $\Delta x$ cannot be decreased by the several orders of magnitude needed for adequate support of all the terms in the Navier-Stokes equation as CPU time, and core storage would become totally impractical. MacCormack (Ref. 11) suggests that the inadequately supported terms are not necessary for boundary-layer flow calculation, but anomalies between the experimental data and the numerical solution show quantitative differences, which could be the results of inadequate mesh resolution in the x-direction.

Additionally, at the hypersonic conditions used in this report, it was necessary to add the damping terms previously discussed to stabilize the solution. These terms, especially in regions of large gradients, could cause "smearing" of the numerical solution as exemplified in Fig. 12. It is not possible to say which of the two effects, grid resolution or damping, caused the discrepancies between the experimental and numerical results. Approximately 6 hr of IBM 370/165 CPU time were required for the above solution.

The last case to be examined is based on VKF Tunnel B conditions and possesses a large separated region. Figure 13 summarizes the tunnel conditions used and presents the results of a time-dependent numerical solution. This solution was generated by computing a hypersonic flat-plate solution and using this solution as initial conditions for the upstream portion of the computational region. Agreement between computed and experimental data was adequate in the region about the peak pressure and good for the pressure gradient near the end of the interaction. The middle portion of the interaction exhibits the correct plateau of pressure. The largest area of disagreement is the beginning of the interaction where the computed plateau and separation regions are much shorter than those indicated by experimental data.

Several attempts were made to rectify the situation, but none were successful. A larger separation region was used in the initial conditions for a subsequent series of runs, but as the solution evolved, the separated region shrank to the initial expanse as seen in Fig. 13. Another attempt was made using input profiles at 0.25 ft from the leading edge instead of 0.50 ft. The final result after some hours of computer time did not differ appreciably from that shown in Fig. 13.

As in the previous case, grid resolution effects and the damping terms effects are cited as being possible causes of the discrepancies between experimental data and the results of the numerical solution. The cell Reynolds numbers $Re_{\Delta y}$ and $Re_{\Delta x}$ possess approximately the same typical values for this case as in the case previously examined. Hence the x-mesh will not adequately support every term in the Navier-Stokes equations. The damping terms were used to stabilize the numerical solution generated for this case. The gradients downstream of the pressure plateau region are larger than the gradients upstream of the plateau region. The values of the damping terms were examined for the entire flow field, and in general, the values in the region downstream
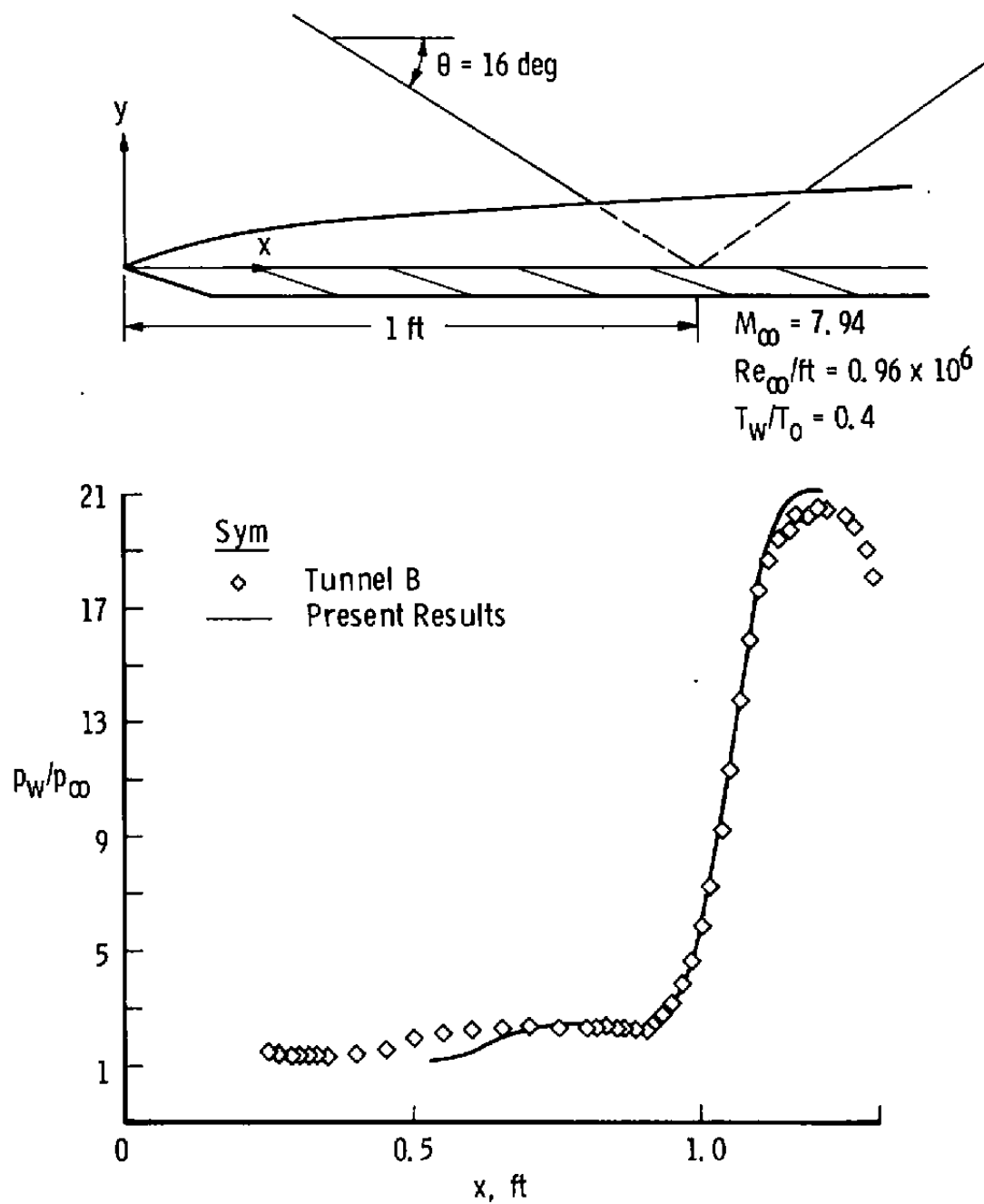
31

Figure 13.  Laminar hypersonic boundary—layer/shock—wave interaction with separated region.

of the pressure plateau were an order of magnitude larger than the values upstream of the pressure plateau. The magnitude of the damping terms in the region upstream of the pressure plateau (in the region about the point of separation) were larger than the remaining portion of the flow field except for the previously delineated downstream region. Thus, the damping terms are of less relative importance within the separated recirculation region, while grid resolution effects are of equal importance. Close to the point of separation, the boundary-layer equations exhibit singular behavior, and within the separated recirculation region, the Navier-Stokes equations hold. It then follows that, within this region, terms not otherwise of importance may be significant. Lack of grid resolution in the x-direction appears to be a likely candidate for the anomalous behavior of the numerical solution. Large separation regions in laminar flow are difficult to predict numerically as evidenced by the results of Skoglund and Gay (Ref. 6) and Hung and MacCormack (Ref. 12). It seems possible that the difficulties encountered with accurate prediction of large separation region are caused by inadequate grid resolution.

Although the region of separation was underpredicted in extent, some interesting information was obtained from the numerical solution. Figure 14 illustrates two velocity profiles: one at separation and one in the separated region. The profile at separation exhibits the expected behavior. The profile within the separated region shows appreciable back flow, a "negative" wall shearing stress, and a substantial height of the separation bubble. The enormous compression that a boundary layer goes through within the interaction is well illustrated by Fig. 15. The streamlines leaving the interaction are compressed to a small fraction of their height entering the interaction. Figure 16 presents streamline patterns for the complete computational region. The initial turning of the flow by the incident shock wave as well as the location of the strong shock wave downstream of the separated region can be seen. Approximately 16 hr of IBM 370/165 CPU time were required to obtain this solution.
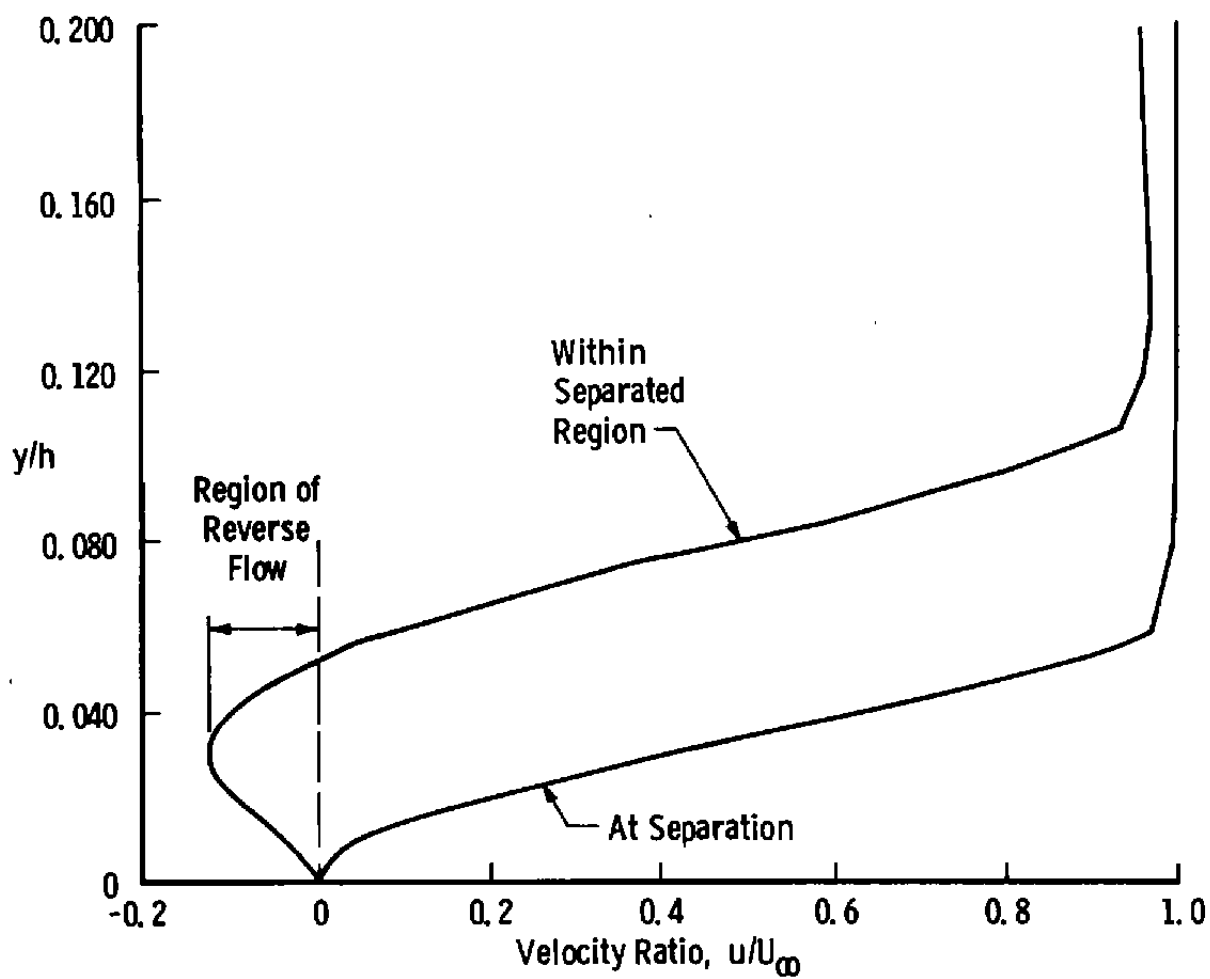
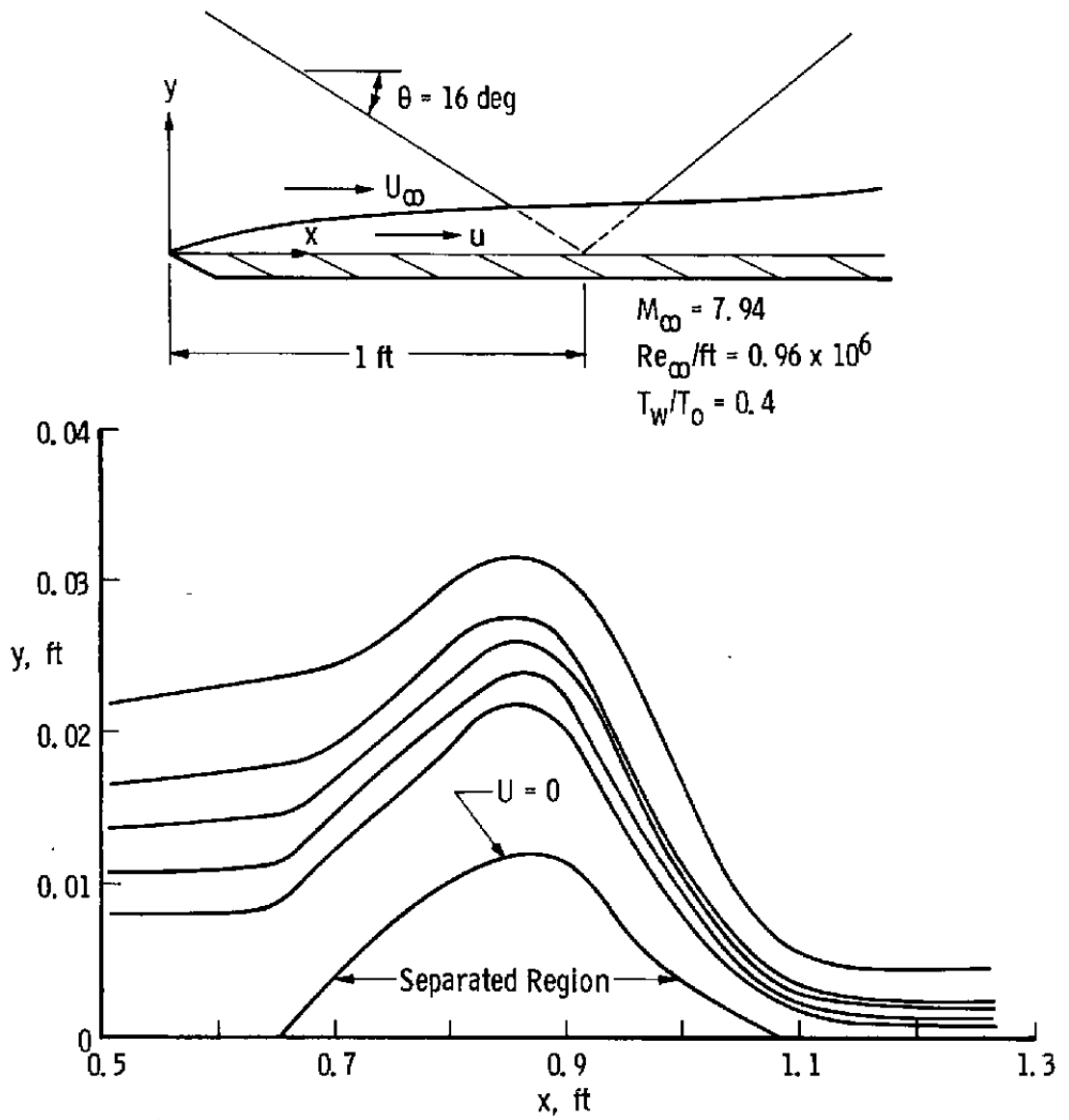Figure 14. Velocity profiles at the point of separation and within the separated region.

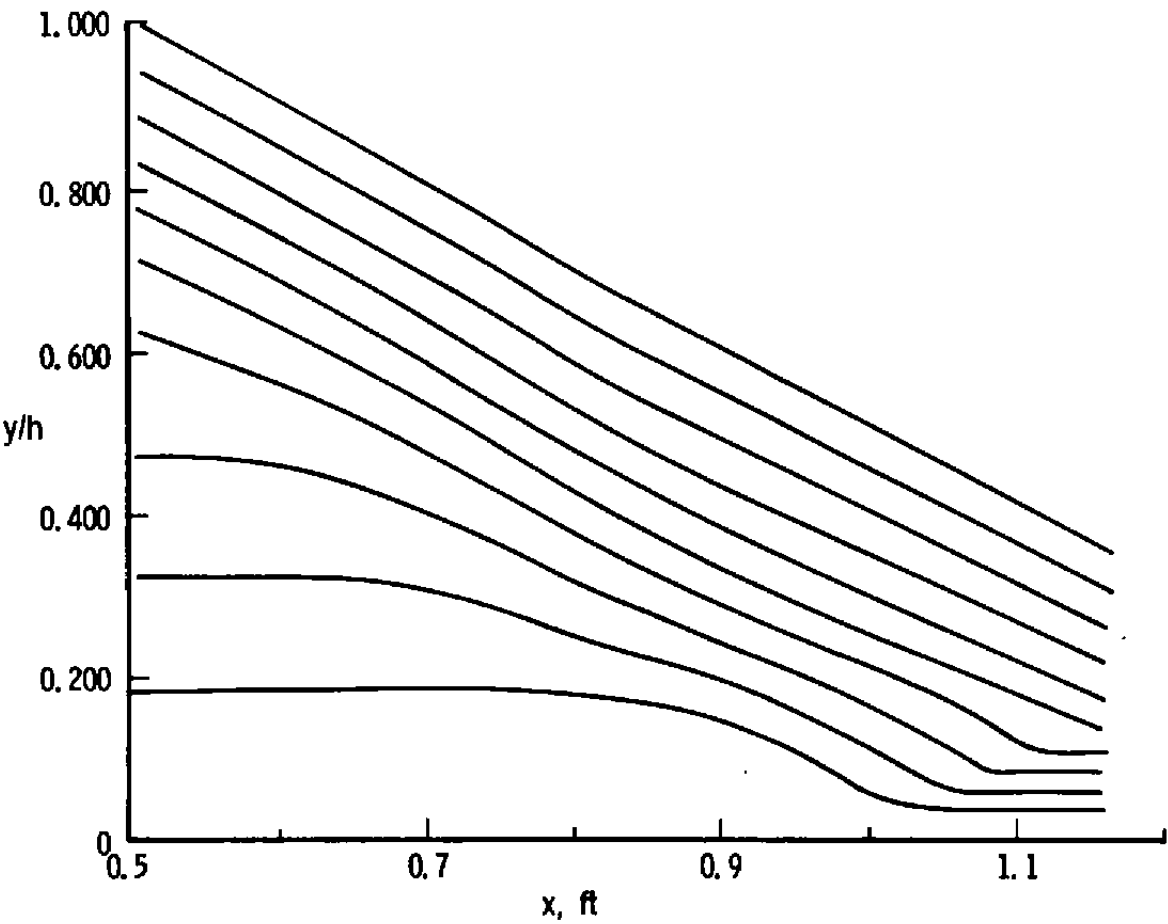Figure 15. Streamlines for hypersonic laminar boundary—layer/shock—wave interaction.

Figure 16. Streamlines for computational region.

# 4.0 CONCLUDING REMARKS

The method of MacCormack has been used to solve numerically the laminar compressible time-dependent Navier-Stokes equations for several boundary-layer/shock-wave interactions in the hypersonic regime. Solutions for each of the interactions were generated using conditions corresponding to available experimental studies. Comparisons of the numerical solutions with experimental data were made to ascertain the validity of the numerical method and to identify regions of anomalous behavior. Possible causes of the anomalies were examined.

The algorithm gave good results when applied to laminar hypersonic interactions that possessed small or no separated regions. The predicted pressure distributions were in excellent agreement with experimental data for cases with small or non-existent separated regions. The predicted wall heat-transfer rates exhibited the correct qualitative trends but not the experimentally measured quantitative values. Overall, the code's performance should be considered as adequate for the prediction of laminar unseparated boundary-layer/shock-wave interactions.

The method, when applied to hypersonic interactions having large separated and recirculating regions, gave marginal performance. The region of separation was underpredicted by a considerable amount although the correct plateau pressure and the correct pressure gradient near the end of the interaction were adequately predicted. Consideration of the effects of damping as well as grid resolution suggested inadequate mesh spacing in the x-direction as the cause.

If inadequate mesh spacing (and the corresponding lack of support for every term of the Navier-Stokes equations) is a prime cause of the cited discrepancies between the numerical results and the experimental data, then the needed reduction of several orders of magnitude in $\Delta x$ would increase CPU time and core storage requirements to untenable levels.

# REFERENCES

1.  MacCormack, R. W. "Numerical Solution of the Interaction of a
    Shock Wave with a Laminar Boundary Layer." Lecture Notes
    in Physics, Vol. 8, Springer-Verlag, New York, 1971, pp.
    151-161.

2.  Roache, P. J. Computational Fluid Dynamics. Hermosa Publishers,
    Albuquerque, New Mexico, 1972.

3.  Richtmyer, R. D. and Morton, K. W. Difference Methods for
    Initial-Value Problems. (Second Edition), Interscience Pub-
    lishers, New York, 1967.

4.  Crocco, Luigi. "A Suggestion for the Numerical Solution of the
    Steady Navier-Stokes Equations." AIAA Journal, Vol. 3,
    No. 10, October 1965, pp. 1824-1832.

5.  Kurzrock, J. W. and Mates, R. E. "Exact Numerical Solutions of
    the Time-Dependent Compressible Navier-Stokes Equations."
    AIAA Paper No. 66-30 presented at the AIAA 3rd Aerospace
    Sciences Meeting, New York, January 24-26, 1966.

6.  Skoglund, V. J. and Gay, B. D. "Improved Numerical Techniques
    and Solution of a Separated Interaction of an Oblique Shock
    Wave and a Laminar Boundary Layer." University of New Mexico
    Bureau of Engineering Research Report ME-41(69)S-068, June
    1969.

7.  MacCormack, R. W. "The Effect of Viscosity in Hypervelocity Impact
    Cratering." AIAA Paper No. 69-354 presented at AIAA
    Hypervelocity Impact Conference, Cincinnati, Ohio, April 30 –
    May 2, 1969.

8.  MacCormack, R. W. and Paullay, A. J.  "Computational Efficiency
    Achieved by Time Splitting of Finite Difference Operators."
    AIAA Paper No. 72-154 presented at AIAA 10th Aerospace Sciences
    Meeting, San Diego, California, January 17-19, 1972.

9.  Baldwin, B. S. and MacCormack, R. W.  "Numerical Solution of the
    Interaction of a Strong Shock Wave with a Hypersonic Turbulent
    Boundary Layer."  AIAA Paper No. 74-558 presented at the AIAA
    7th Fluid and Plasma Dynamics Conference, Palo Alto,
    California, June 17-19, 1974.

10. Baldwin, B. S. and MacCormack, R. W.  "Interaction of Strong Shock
    Wave with Turbulent Boundary Layer." Lecture Notes in Physics,
    Vol. 35, Springer-Verlag, New York, 1975, pp. 51-56.

11. MacCormack, R. W. and Baldwin, B. S.  "A Numerical Method for
    Solving the Navier-Stokes Equations with Application to
    Shock-Boundary Layer Interactions."  AIAA Paper No. 75-1 presented
    at the AIAA 13th Aerospace Sciences Meeting, Pasadena,
    California, January 20-22, 1975.

12. Hung, C. M. and MacCormack, R. W.  "Numerical Solutions of Supersonic
    and Hypersonic Laminar Flows over a Two-Dimensional Compression
    Corner."  AIAA Paper No. 75-2 presented at AIAA 13th Aerospace
    Sciences Meeting, Pasadena, California, January 20-22, 1975.

13. Baldwin, B. S., MacCormack, R. W., and Deiwert, G. S.  "Numerical
    Techniques for the Solution of the Compressible Navier-Stokes
    Equations and Implementation of Turbulence Models."  Paper 2
    in "Computational Methods for Inviscid and Viscous Two-and-
    Three-Dimensional Flow Fields."  AGARD Lecture Series Pre-Print
    No. 73, 1975.

14. Baldwin, B. S. and Rose, W. C. "Calculation of Shock-Separated Turbulent Boundary Layers." Paper 12 in "Aerodynamic Analyses Requiring Advanced Computers." NASA SP-347, Conference held at NASA Langley Research Center, Hampton, Virginia, March 4-6, 1975, pp. 401-417.

15. Deiwert, G. S. "Numerical Simulation of High Reynolds Number Transonic Flows." AIAA Paper No. 74-603, presented at AIAA 7th Fluid and Plasma Dynamics Conference, Palo Alto, California, June 17-19, 1974.

16. Deiwert, G. S. "Computation of Separated Transonic Turbulent Flows." AIAA Paper No. 75-829 presented at the AIAA 8th Fluid and Plasma Dynamics Conference, Hartford, Connecticut, June 16-18, 1975.

17. MacCormack, R. W. "Numerical Methods for Hyperbolic Systems." Presented at the Short Course on Advances in Computational Fluid Dynamics, The University of Tennessee Space Institute, Tullahoma, Tennessee, December 10-14, 1973.

18. Horstman, C. C., Kussoy, M. I., Coakley, T. J., Rubesin, M. W., and Marvin, J. G. "Shock-Wave-Induced Turbulent Boundary-Layer Separation at Hypersonic Speeds." AIAA Paper No. 75-4 presented at the AIAA 13th Aerospace Sciences Meeting, Pasadena, California, January 20-23, 1975.

19. Haslett, R. A., Kaufman, L. G., II, Romanowski, R. F., and Urkowitz, M. "Interference Heating Due to Shock Impingement." AFFDL-TR-72-66, July 1972.

20. Zumwalt, G. W. "Weak Wave Reflections at near 90 deg of Incidence." Tran. ASME, Journal Applied Mechanics, Vol. 41, Series E, No. 4, December 1974, pp. 1142-1143.

21. Carter, J. E. "Numerical Solutions of the Navier-Stokes Equations for the Supersonic Laminar Flow over a Two-Dimensional Compression Corner." NASA TR R-385, July 1972.

22. Grossman, B. and Moretti, G. "Time-Dependent Computation of Transonic Flows." AIAA Paper No. 70-1322 presented at AIAA 7th Annual Meeting and Technical Display, Houston, Texas, October 19-22, 1970.

23. Kaufman, L. G., II, and Johnson, C. B. "Weak Incident Shock Interactions with Mach 8 Laminar Boundary Layers." NASA TN D-7835, December 1974.

24. Cheng, S. I. "A Critical Review of the Numerical Solution of Navier-Stokes Equations." Princeton University Department of Aerospace and Mechanical Sciences Report No. 1158, February 1974.

## NOMENCLATURE

$C_v$         Constant volume specific heat, $4,290 \ ft^2/sec^2-°R$

c          Local speed of sound

e          Total internal energy per unit volume

F          Column vector containing convection and diffusion fluxes
           in the x-direction defined by Eq. (3)

G          Column vector containing convection and diffusion fluxes
           in the y-direction defined by Eq. (4)

h          Height of computational grid, ft

$h_f$         Height of fine mesh portion of computational grid, ft

IMAX       Total number of mesh points in the x-direction

JMAX       Total number of mesh points in the y-direction

k          Thermal conductivity

L          Location of shock impingement point on flat plate

Lx         Operator denoting MacCormack algorithm x-direction
           contribution defined by Eqs. (8) and (9)

Ly         Operator denoting MacCormack algorithm y-direction
           contribution defined by Eqs. (10) and (11)

M          Fine grid passes for each course grid pass defined by
           Eq. (25)

$M_\infty$       Free-stream Mach number

p       Static pressure

Re       Reynolds number

$Re_{\Delta x}$       Cell Reynolds number for x-mesh defined by Eq. (27)

$Re_{\Delta y}$       Cell Reynolds number for y-mesh defined by Eq. (26)

$St_\infty$       Stanton number based on free-stream conditions and adiabatic wall temperature

T       Static temperature

t       Time

U       Column vector of conserved quantities per unit volume defined by Eq. (2)

u       Component of velocity in the x-direction

v       Component of velocity in the y-direction

x       Coordinate along plate surface

y       Coordinate normal to plate surface

$\Delta F$       Damping term in Lx operator used to stabilize calculation defined in Eq. (19)

$\Delta G$       Damping term in Ly operator used to stabilize calculation defined in Eq. (18)

$\Delta t$           Time step used in temporal advancement

$\Delta x$           Mesh spacing in x-direction

$\Delta y$           Mesh spacing in y-direction

$\gamma$           Ratio of specific heats, 1.4

$\lambda$           Coefficient of bulk viscosity, taken as $-2/3\ \mu$

$\mu$           Molecular viscosity coefficient

$\rho$           Mass density

$\sigma_x, \sigma_y$           Normal stress fluxes in Navier-Stokes equations defined by Eqs. (5) and (7)

$\tau_{xy}, \tau_{yx}$           Shear stress fluxes in Navier-Stokes equations defined by Eq. (6)

## Subscripts

1           Upstream of incident shock

2           Downstream of incident shock and upstream of reflected shock

3           Downstream of reflected shock

c           Denotes coarse grid

f           Denotes fine grid

i           General grid point in x-direction

j          General grid point in y-direction

w         Evaluated at wall

x         x-direction

y         y-direction

o         Stagnation or total

$\infty$       Free stream

## Superscript

n         Time level

——      Evaluated during corrector pass using predictor values